*Solid State Science and Technology, Vol. 12, No. 1 (2004) 166-176*

# CHARACTERISTICS OF CHARGED SPRAYS OF INSULATING HYDROCARBON LIQUIDS

Andrew R.H Rigit[1], John S. Shrimpton

[1]*Faculty of Engineering, University of Sarawak, 94300 Kota Samarahan, Sarawak, Malaysia.*
*arigit@feng.unimas.my*
*Department of Mechanical Engineering, Imperial College London, Exhibition Road, London SW7 2BX, England, UK.*
*j.shrimpton@ic.ac.uk*

## ABSTRACT

This paper describes the characteristics of charged sprays of insulating liquids generated by charge injection electrostatic atomizers, assessed for a smaller range of orifice diameter and a more viscous liquid than previously investigated. The jet break-up dynamics are qualitatively studied with a high-speed video camera, and the general spray characteristics are quantitatively described in terms of droplet velocity and diameter pdfs with a phase Doppler anemometry (PDA). A purpose-built transmitter and receiver, and a purpose-built signal-processing counter are used as the main PDA component. Spray charge and mass flow rate as a function of spray radius is also studied using a purpose-built collecting system, and the results suggest that highly charged droplets exist outside the spray cone.

## INTRODUCTION

Charge injection atomizers, based on the point to plane geometry, can generate electrically charged sprays of insulating hydrocarbon liquids, and have been developed and refined in the recent past [1-3]. The technique has distinct advantages over conventional atomization techniques as sprays may be produced without modifying the electrical properties of the liquid or using secondary methods such as air blast. The introduction of electric charge to a liquid jet will normally destabilize the jet surface by overcoming the balancing force of the liquid surface tension [4], and thus promoting atomization efficiency. This usually leads to smaller mean droplet diameters and larger spray cone angles due to space charge induced repulsion of like charged droplets resulting in good inter-phase mixing. Thus, electrically charged sprays have the unique benefits of lack of droplet agglomeration, low droplet concentration, as well as controllable droplet size distribution, spray plume shape and droplet mass flux distribution.

Phase Doppler Anemometry (PDA) has been used for charged spray characterization [5-10]. Dunn and Snarski [6] examined the spray of ethanol drops of diameter range 1-50 μm using PDA and found evidence of proportionality between droplet charge and diameter. In a later work, Gomez and Tang [7] used PDA to correlate the droplet velocity and size information. They showed that the droplet diameter decreased as applied voltage increased and higher flow rates had larger droplet diameters due to lower average specific charges, as the current supply was limited. Gomez and Tang [8] show a development of bimodal size distributions from an initially unimodal one because of the ejection of nearly monodisperse secondary atomization products from the parent droplets. Shrimpton and Yule [10] used PDA and

Malvern particle sizer to measure droplet velocity and size distributions and a similar bimodal character of the size distribution, using charge injection atomizers of large orifice diameter, $d$ = 500 μm, was shown. Their results show the difficulties introduced when applying the PDA technique to sprays containing ligaments and large droplets that may be non-spherical. In the work of Shrimpton and Yule [11], for orifice diameter, $d$ = 250 μm, electrostatically charged sprays of kerosene were found to contain relatively large numbers of small droplets.

The combination of both larger surface electrical forces due to surface charge and more significant aerodynamic shear [12] at higher liquid injection velocity $u_{inj}$ improves atomization performance. The small droplets were more likely to strongly repel away from the core region where the radial electric field component, due to the spray specific charge was most intense. The larger droplets are more likely to be found near to the spray centre line since they typically have much more significant inertia. These two factors, taken together cause a radial stratification of the average droplet diameter to occur, with average droplet diameter reducing with increasing displacement away from the axis. The objective of this paper is to study the effects of orifice diameter $d$, injection velocity $u_{inj}$, spray specific charge $Q_V$ and liquid physical properties on the spray characteristics. This study extends previous studies [2, 11] to atomizers with a smaller range of orifice diameters and more viscous liquids than previously examined.

## EXPERIMENTAL DETAILS

The design and operating characteristics of charge injection atomizers, used to generate the charged spray plume is given elsewhere [1-2, 13-14] and is briefly explained here. A stainless steel sewing needle with a sharp tip, connected to a Spellman Model LS30PN high voltage power supply, acts as a cathode inside the atomizer nozzle for charging the spray. The spray current $I_S$ was defined as the current that exits the atomizer and carried away by the charged spray. The leakage current $I_L$ was defined as the current that passed across the liquid inside the nozzle to the earthed inner surfaces of the nozzle body and earth. The total current, $I_T$ was calculated as the sum of the spray current $I_S$ and the leakage current $I_L$, assuming that the liquid upstream of the nozzle acted as a perfect insulator and that the needle and the nozzle body were perfectly isolated from the rig supports and earth. The Keithley Model 6514 electrometer was used throughout the work and the electrometer reading is rated as having an accuracy of ± 0.1%. Compressed air from a pressurized cylinder was used for inducing liquid flow in the system. A Brooks Sho-rate® Flowmeter Model 1350 was installed to monitor liquid flow rates, $\dot{\tau}$. The spray specific charge $Q_V$ is defined as the quotient of the spray current $I_S$ and the liquid flow rate $\dot{\tau}$.

The images of the unstable jet were obtained with a Kodak Extapro Model 4540 high-speed video camera by using the highest frame rate available of 27,000 and 40,500 frames/second. A Leica Monozoom 7 lens with a magnification factor of 46.9 μm/pixel was fitted onto the camera to focus an area of 3×3 mm$^2$ downstream of the atomizer nozzle and coaxial with the liquid jet exiting the orifice. A 50 W halogen light was used as an illumination source and was positioned horizontally in front of the jet and the camera. To characterize the spray in terms of droplet size and velocity distributions, the phase Doppler anemometry technique was used. An in-house transmitter, receiver and signal-processing counter were used [15-16]. A

Spectra Physics argon-ion laser beam was focused onto the surface of a circular diffraction grating, which acts as a beam splitter and could be rotated at a set angular speed to provide a frequency shift between the two beams for the resolution of directional ambiguity in velocity. The rotating diffraction grating divided the incident beam into two-equal intensity beams. An intersection volume was formed using a set of collimating and focusing lenses. The scattered light was focused to the centre of a slit to provide an effective length of the measuring volume and was passed through a mask with three evenly spaced rectangular apertures to three Hamamatsu Model R1477 photodetectors. The laser and the transmitter were both securely mounted and precisely aligned relative to each other on a fixed optical bench. The receiver was securely mounted on a separate rail at a 30 degrees scattering angle. Fig. 1 shows the schematic of the PDA system.

Spray charge and mass flow were measured using a purpose-built collecting system made from a set of electrode rings which varied in diameter designed in such a way that it would be possible to measure the charge-to-mass ratio as a function of spray radius. The system was made of a set of stainless steel tubes of non-uniform spacing to obtain a nominally constant mass flow rate of liquid for each of the annuli as shown in Figs. 2(a).

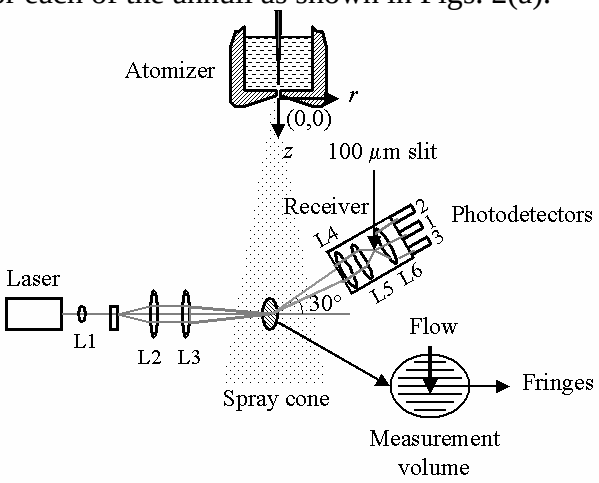


Figure 1 A schematic of the PDA optical arrangement.

In order to measure and differentiate the spray current carried by spray droplets that will enter each of the annulus, the surface of the annulus has been separated from each other by an electrically insulating silicone conformal coating (SCC). The SCC was thermal cured for two hours at 100° C before being coated by an electrically conductive nickel coating. The schematic of the coated electrode ring surface is shown in Fig. 2(b). The interface resistance of the silicone coating prior to adding the conductive layer was measured using the electrometer and found to be higher than 200GΩ. A set of webs was used to hold the outer tubes together and a constant blockage factor of 0.8 is applied on each of the annulus due to the introduction of the webs. Thinly lined wire wool was also placed inside the annulus to ensure a good and fast electrical response. A method to collect and weigh the liquid flows through each annuli was devised and tested, and found to be accurate to within 12.5% of the total mass flow rate.

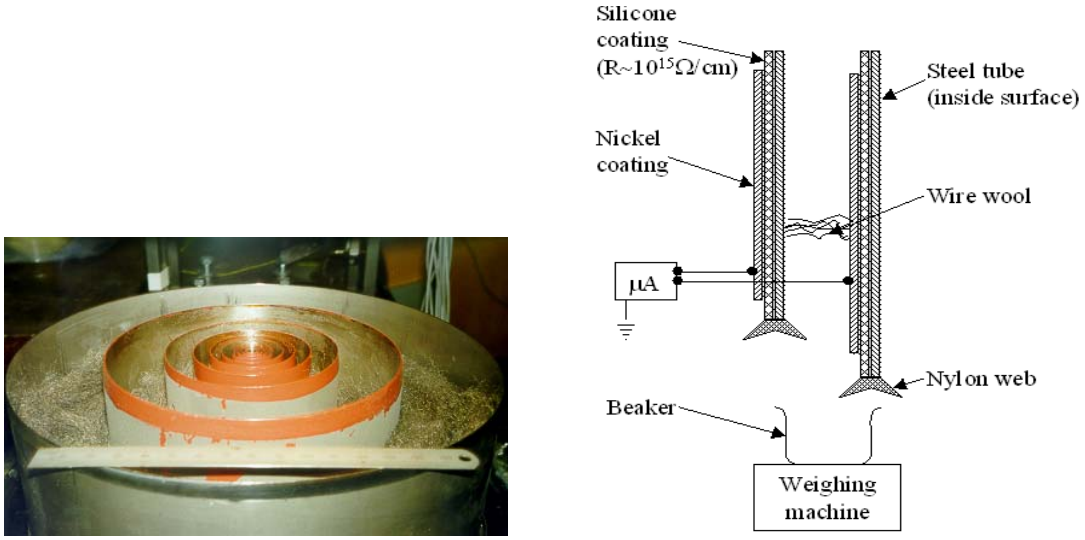


Figure 2. (a) Picture of earthed stainless steel electrode rings with a 150 mm steel rule as a scale and (b) the schematic of the coated electrode ring surface.

**Visualization Results**

The jet break up dynamics was studied using the high-speed camera and the monozoom lens. In Figs. 3(a) – (h), a distorted Rayleigh jet break-up as previously observed in reference [4] is evident. The figures show sequential images of the charged liquid jet for nozzle orifice diameter $d$ = 116 μm and liquid injection velocity $u_{inj} \approx 6$ m/s, flowing from right to left, with spray specific charge $Q_V \approx 2.29$ C/m$^3$. The time interval between two consecutive frames is $t_i$ = 0.123 ms with an exposure time per frame of $t_e$ = 0.025 ms. The centre of the image is 1.5 mm from the nozzle orifice plane, which is on the right side of the image and is just visible. As the spray develops from Figs. 3(a) – (h) pronounced perturbation and good drop dispersal were observed, with droplet diameters estimated from the images to be $D \approx 2.35d \approx 273$ μm. The atomization is however, highly regular, and has the possibility of producing near mono-size spray plumes.

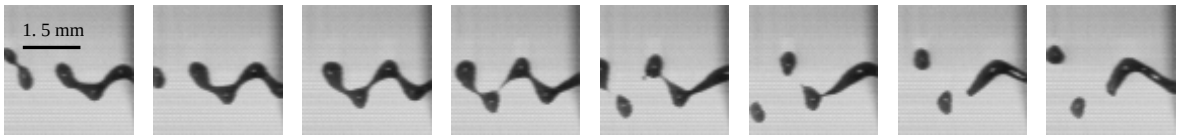


Figure 3. Jet break-up dynamics for $d$ = 116 μm, $u_{inj} \approx 6$ m/s, $Q_V \approx 2.29$ C/m$^3$, $t_e$ = 0.025 ms, $t_i$ = 0.123 ms.

Increasing the jet velocity produces a more chaotic jet break-up process. Figs. 4(a) – (h) show a charged liquid jet with $u_{inj} \approx 15$ m/s and $Q_V \approx 3.16$ C/m$^3$. Droplet development starts with the collapse of the charged cylindrical jet into a thick-rimmed, ribbon-like structure as the jet emerges from the nozzle as have been previously observed using the Spray Triode (ST) [3] using a viscous mineral oil at $u_{inj} \approx 2.4$ m/s and $Q_V \approx 1.5$ C/m$^3$. The charged cylindrical jet becomes unstable due to the growth of an initial surface wave instability is augmented by the space charge repulsion of the like charges contained within it and on the liquid jet. As the ligaments emerge from the liquid jet, they quickly lose their forward momentum to aerodynamic drag and thus appear to curve towards the earthed nozzle surface. The ligament

tips collect liquid and they break-up via Rayleigh type instability to produce rapidly dispersing droplets. From the above discussion of jet break-up dynamics, it is clear that jet break-up and droplets dispersal at atmospheric pressure and room temperature are strongly effected by $u_{inj}$ and to some extent, by $Q_V$.

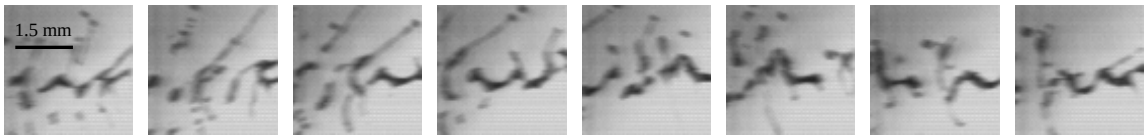


**(a)** $t_1$ = 0s **(b)** $t_2$ **(c)** $t_3$ **(d)** $t_4$ **(e)** $t_5$ **(f)** $t_6$ **(g)** $t_7$ **(h)** $t_8$

Figure 4. Jet break-up dynamics with the right side of the frame at a distance 1.5 mm downstream from the nozzle plane for $d$ = 116 μm, $u_{inj} \approx$ 15 m/s, $Q_V \approx$ 3.16 C/m$^3$, $t_e$ = 0.025 ms, $t_i$ = 0.123 ms.

**Phase Doppler Anemometry Results**

The qualitative droplet formation process from Rayleigh-like ligament disintegration produces charged spray plumes and these have been characterized with PDA. Four characteristic sprays defined in table 1 are discussed. Each of the conditions defined in table 1 gives sprays of different character with different mean spray specific charge $Q_V$ for each atomizer emitting electrode voltage $V$ applied. Each of the sprays was approximately at the maximum $Q_V$ for the given bulk injection velocity $u_{inj}$. The test liquid used was diesel calibration fluid.

Table 1. Spray operating conditions.

| Case | Symbol | $D$ (μm) | $u_{inj}$ (m/s) | $\dot{m}$ (g/s) | V (kV) | $Q_V$ (C/m$^3$) |
|---|---|---|---|---|---|---|
| (i) | λ | 254 | 10 | 0.4115 | 10 | 1.13 |
| (ii) | ν | 140 | 10 | 0.1304 | 9 | 2.25 |
| (iii) | σ | 140 | 15 | 0.1875 | 11 | 2.67 |
| (iv) | υ | 116 | 15 | 0.1263 | 10 | 3.16 |

The spray for case (i) in table 1 will be compared with existing data sets for kerosene [2, 11], using an atomizer of orifice diameter $d$ = 250 μm and $V \approx$ 10 kV, at $u_{inj} \approx$ 10 and 34 m/s, $\dot{m} \approx$ 0.4 and 1.336 g/s, and $Q_V \approx$ 1.2 and 1.8 C/m$^3$ respectively. The PDA data is first described and the resulting discussion is separated into three sections to identify the effect of the named parameters. From the PDA measurement data, the droplet mean and rms axial $u_i$ and radial $v_i$ velocity components, diameter $D_i$, number of droplets $n_i$ for each of the droplet size class $i$ are presented. The droplet diameter was divided into nine size classes $i$ = 1:9 of equal width of 42 μm in an interval of $0 \le D \le 378$ μm. The diameter $D_i$ is the midpoint diameter for the $i^{th}$ size class.

**Spray Characterization along Selected Spray Radii**

**Effect of increasing $u_{inj}$ at constant $d$ and maximum $Q_V$**

The effect of bulk injection velocity on droplet formation from a nozzle with orifice diameter $d$ = 140 μm at $u_{inj} \approx$ 10 and 15 m/s with $Q_V$ = 2.25 and 2.67 C/m$^3$, denoted by symbol (ν) and (σ) respectively in Fig. 5 is investigated. Fig. 5 reveals the key dynamics of the polydispersed charged spray plume. In this and subsequent figures, the spray radius $r$ has been normalized by the orifice diameter $d$. At $z$ = 30 mm, since the largest droplets retain a significant fraction of their axial momentum, and probably posess smaller charge to mass ratios, these droplets

populate the centreline region. This is supported by the observation that the mean axial velocity profile, as a function of *r/d* is strongly peaked on the centreline at *z* = 30 mm.

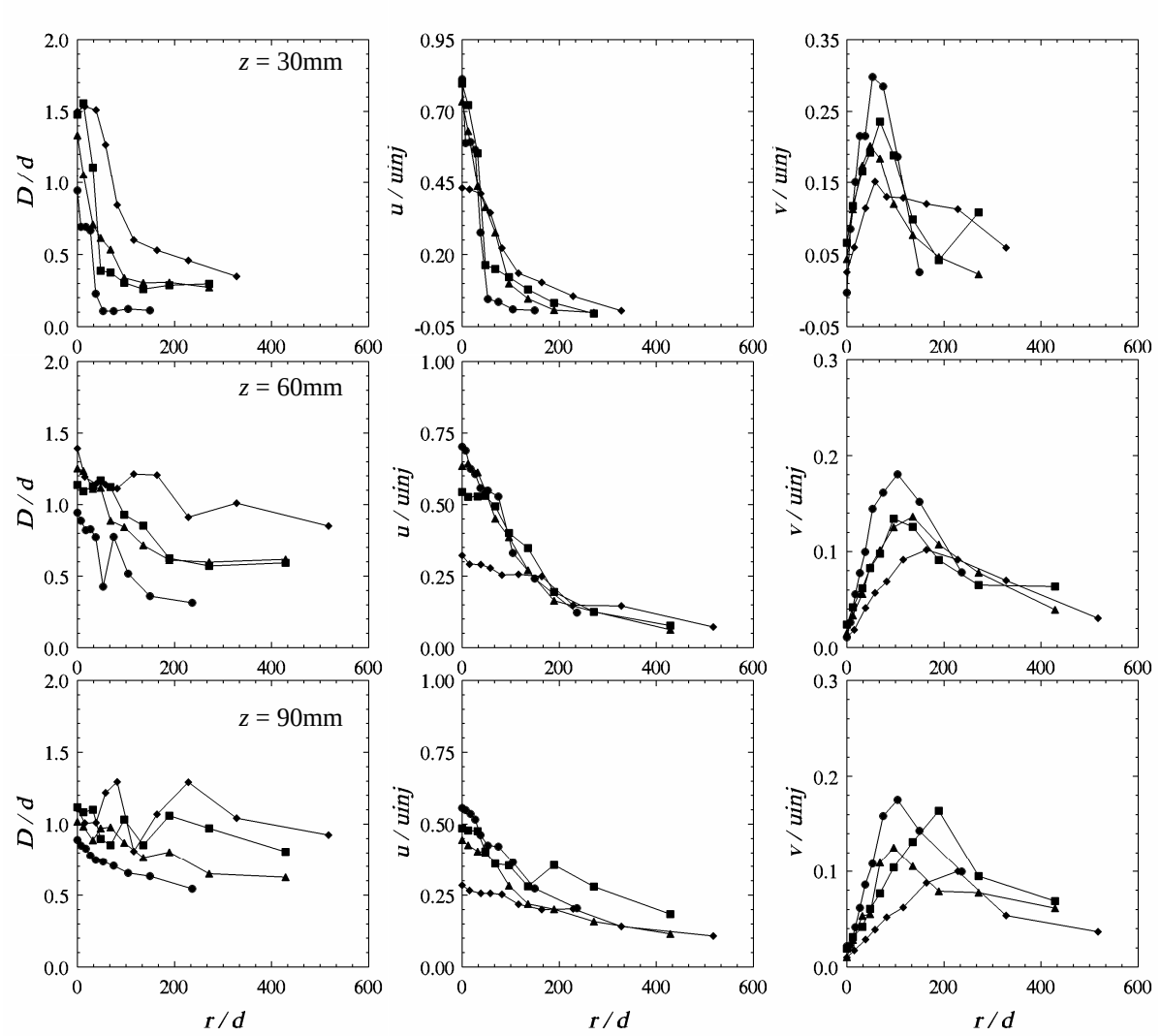


Figure 5. Variation of (a) droplet diameter $D_{10}$, (b) mean axial *u* and (c) mean radial *v* velocity components with radial displacement *r/d* at axial displacement *z* = 30, 60 and 90 mm for spray case (i) $d$ = 254 μm, $u_{inj} \approx$ 10 m/s and $Q_V$ = 1.13 C/m$^3$ (λ), (ii) $d$ = 140 μm, $u_{inj} \approx$ 10 m/s, $Q_V$ = 2.25 C/m$^3$ (ν), (iii) $d$ = 140 μm, $u_{inj} \approx$ 15 m/s, $Q_V$ = 2.67 C/m$^3$ (σ), and (iv) $d$ = 116 μm, $u_{inj} \approx$ 15 m/s and $Q_V$ = 3.16 C/m$^3$ (υ).

For $r/d$ > 100, most of the droplets present are small, i.e. $D_i/d$ < 0.5, and therefore it is these droplets that possess significant charge-to-mass ratios and contribute to the radial velocity profile, created by the space charge replusion within the spray plume. As the spray evolves further downstream, i.e. at *z* = 60 and 90 mm as shown in Fig. 5, all droplet size classes diffuse radially, contributing to a broadening of the profile of $D_{10}/d$ and $u/u_{inj}$. An initial rise in the radial velocity profiles is thought due to the electric field shape produced by the symmetry of the spray plume. The mean radial velocity components at the spray centre should equal zero due to the spray axisymmetry and this is shown in Fig. 5 for both sprays. The radial electric field is at its maximum near but not at the spray axis and decreases rapidly as radial displacement increases. Thus, it is expected the radial velocity profile should

correspond to the shape the radial electric field profile since the droplet momentum relaxation times are short compared to the time taken for a droplet to get from the axis to the spray edge.

**Effect of reducing *d* at constant $u_{inj}$ and maximum $Q_V$**

The effect of reducing the orifice diameter *d* is now discussed by presenting a subset of data presented earlier. The aim of these comparisons is to define the degree of influence of *d* has on droplet formation.

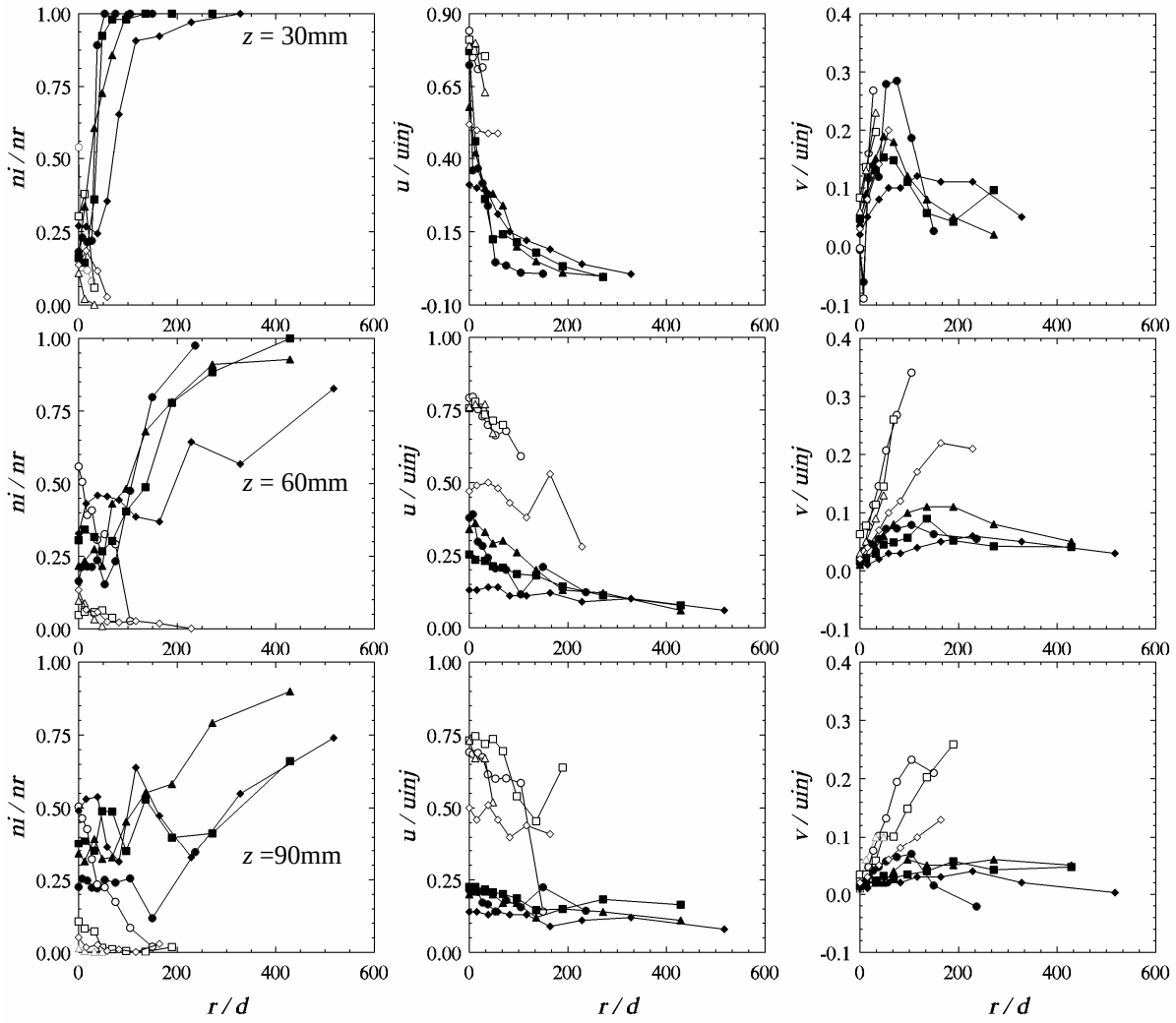


Figure 6. Variation of (a) droplet number for $D_i < 126$ μm (solid points) and $D_i > 252$ μm (hollow points), and mean (b) axial *u* and (c) radial *v* velocity components with radial displacement *r/d* at axial displacement *z* = 30, 60 and 90 mm for spray case (i) *d* = 254 μm, $u_{inj} \approx 10$ m/s and $Q_V = 1.13$ C/m$^3$ (λ), (ii) *d* = 140 μm, $u_{inj} \approx 10$ m/s, $Q_V = 2.25$ C/m$^3$ (ν), (iii) *d* = 140 μm, $u_{inj} \approx 15$ m/s, $Q_V = 2.67$ C/m$^3$ (σ), and (iv) *d* = 116 μm, $u_{inj} \approx 15$ m/s and $Q_V = 3.16$ C/m$^3$ (υ).

As in the previous discussion on the effect of increasing $u_{inj}$ at constant *d*, the droplet diameter is shifted to smaller $D_{10}$ as *r/d* increases, giving a distinct droplet size plateau with the smaller droplets become more numerous. The droplet size also plateau out a higher *r/d* ratio as *z* increases as the large droplets spreading out. The axial and velocity profiles also reduce as *r/d* increases, with high axial velocities occur in the spray centre. For case (iv), the lower axial velocities at the spray centre indicate a lower initial momentum for sprays from

smaller orifice diameter, and further reduced by the existence of numerous small droplets as one would expect. The PDA will not pick up all droplets on the spray axis as the droplets are moving faster and are more numerous, giving a more scattered light.

The existence of small and large droplets which influence the velocity profiles may be investigated by plotting the velocity profiles and droplet pdfs $n_i/n_r$ for two droplet size classes of small ($D_i < 126$ μm) and large ($D_i > 252$ μm) respectively as shown in Fig. 6 for spray case (i) – (iv). Overall, the result in Fig. 6 confirms that the large droplets occupy a narrow core of relatively high velocity and the smaller droplets have a more uniform mean velocity distribution and are the main constituent of the outer region as previously observed for kerosene sprays [11]. As for the spray in case (i), the number of droplet for $D_i > 252$ μm is relatively high at the spray core, i.e. $r/d = 0$. This observation may infer that the main constituent of droplets at this region is the large droplet which are perhaps jet ligament that yet to break-up into droplets. However, as $r/d$ and $z$ increase, the number of this large droplet reduces and the number of small droplet increases, which infer that the droplet break-up processes are taking place over the relatively small time scale. The increase in the number of the small droplet is also enhanced by the fact that the small droplet being repelled away from the spray core.

**Effect of liquid physical properties**

The effect of liquid physical properties on droplets trajectory for charged spray is now investigated. The results of the present study for case (i) in table 1 is compared with kerosene from a previous study by Shrimpton and Yule [11] of two sprays with $Q_V \approx 1.2$ and 1.8 C/m$^3$ for $d = 250$ μm. Fig. 7 shows the profiles of mean axial and radial velocity components and droplet size $D_{10}$ for the sprays. The data for case (i) for $Q_V \approx 1.13$ C/m$^3$ for $d = 254$ μm from Fig. 5 is included here for comparison.

From Fig. 7, similar trends as discussed previously are observed in the $D_{10}$ and both and radial velocity profiles. For the kerosene spray with $u_{inj} \approx 34$ m/s and $Q_V = 1.8$ C/m$^3$, a much narrowing spray cone is observed in the $u/u_{inj}$ velocity profiles for $z > 30$ mm. However, at spray axis, i.e. $r/d = 0$, the peak $u/u_{inj}$ ratio scales well for all three cases. There is some dependence on axial variations that may be due to the more viscous oil breaking up more slowly as shown by the similar droplet size at the spray periphery, where they take longer to form and the jet break-up lengths may be different. Thus, it could be concluded that liquid physical properties over the very small range we have looked at (for $780 \le \rho \le 815$ kg/m$^3$, $0.0008 \le \mu \le 0.0026$ kg/ms, $0.0225 \le \sigma_T \le 0.0250$ Ns/m$^2$) do not have much effect on the droplet radial dispersion rates and $D_{10}$ profile, and this effect could be discounted when analyzing the charge-to-mass ratio. However, from the result of kerosene with $Q_V \approx 1.8$ C/m$^3$, it can be concluded that highly charged spray will have smaller droplet size due to the breaking up of the droplet as described in the previous two sub-sections 4.2.1 and 4.2.2.

**Annular Mass and Current Flux Measurements**

Spray charge and mass flow were measured as a function of spray radius at $z = 100$ mm using the purpose-built collecting system described earlier. Four spray cases in table 1 are further investigated by evaluating spray mass and charge flux as a function of spray radius. The liquid flow into each of the annular of the electrode rings set was collected over a period of time $t$ and weighed. For spray cases (ii) – (iv) in table 1, with nozzle orifice diameter $d = 116$

and 140 μm, a maximum collection time of $t$ = 14 minutes was imposed due to a built-up of carbon deposit on the nozzle surface around the orifice exit. The restriction was due to the fact that the electrical performance, and hence the atomization and therefore spray steadiness may be compromised by the carbon built-up. For $d$ = 254 μm in spray case (i) in table 1, the collection time was shortened to $t$ = 4 minutes due to a higher mass flow rate $\dot{m}$ at the tested bulk injection velocity $u_{inj} \approx$ 10 m/s, where $\dot{m}$ is approximately 3× higher than the lowest $\dot{m}$ as in spray case (iv). Overall, a moderate accuracy with underestimation ranging from 0.1 – 7.5% is obtained.

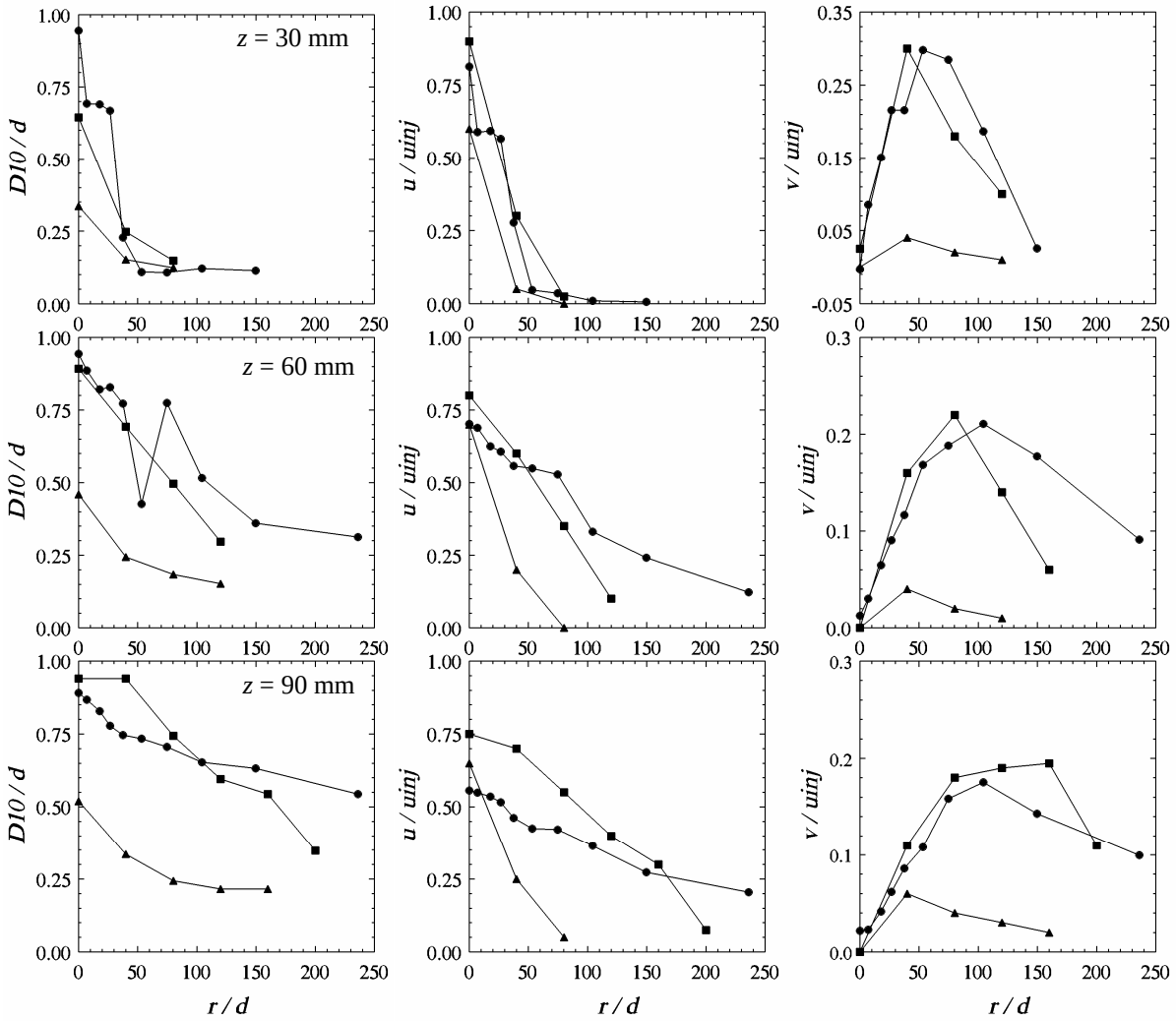


Figure 7. Variation of (a) droplet diameter $D_{10}$, (b) mean axial $u$ and (c) mean radial $v$ velocity components with radial displacement $r/d$ at axial displacement $z$ = 30, 60 and 90 mm for spray case (i) $d$ = 254 μm at $u_{inj} \approx$ 10 m/s and $Q_V$ = 1.13 C/m$^3$ (λ) with diesel calibration fluid; and from Shrimpton and Yule [11] with kerosene for $d$ = 250 μm at (ii) $u_{inj} \approx$ 10 m/s and $Q_V$ = 1.2 C/m$^3$ (ν) and (iii) $u_{inj} \approx$ 34 m/s, $Q_V$ = 1.8 C/m$^3$ (σ).

The division of mass and current *rates* will give the spray specific charge as a function of radius, i.e. $Q_V(r) = \dot{m}(r)/I_S(r)$. Fig. 8 shows the variation of annular spray specific charge versus radial position of the annulus centre from the spray axis, by dividing the data of annular spray current with mass flow rate. The annular spray specific charge is normalized by each of the spray mean specific charge as previously summarized in table 1. Generally, the

plot shows a strong trend of increasing 'spray' specific charge as the normalized radial position *r/d* increases, inferring that the highly charged droplets are repelled away from the spray core. This trend suggests that the maximum charge for a droplet size class $Q_{max,i}$ is more likely to be found at the maximum radial displacement $r_{max}$. However, the increment is becoming less pronounced as the 'net' radial momentum gain increased. This may infer that the charges are well distributed within the spray via further break-up of the droplets into smaller droplets. This is confirmed with the diameter pdfs discussed previously in section 4.2, as the droplet pdfs increases for smaller droplets further away from the spray axis, and the trend is getting more dominant as $Q_V$ increased.

It is also observed in Fig. 8 that the normalized annular spray specific charge is higher near to the spray core at a higher bulk injection velocity $u_{inj}$ for $d$ = 140 μm, spray case (iii). However, further away from the spray axis, the normalized annular spray specific charge is relatively higher at a lower $u_{inj}$, case (ii). These two opposite trends confirm that the highly charged droplets travel only a short distance in the radial direction at a higher $u_{inj}$ since the axial momentum is more dominant. At a lower $u_{inj}$, the droplets take a relatively longer distance to travel further in the radial direction due to lower spray axial momentum.

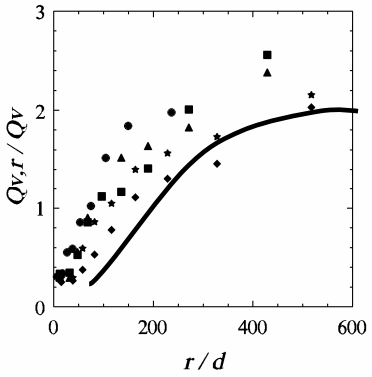


Figure 8. Variation of normalized annular spray specific charge $Q_{V,r}/Q_V$ versus normalized radial position of annulus centre from spray axis *r/d* at an axial position *z* = 100 mm downstream of the nozzle from direct measurements of spray mass flow rate into each annulus for spray case (i) $d$ = 254 μm, $u_{inj} \approx$ 10 m/s and $Q_V$ = 1.13 C/m$^3$ (λ), (ii) $d$ = 140 μm, $u_{inj} \approx$ 10 m/s, $Q_V$ = 2.25 C/m$^3$ (ν), (iii) $d$ = 140 μm, $u_{inj} \approx$ 15 m/s, $Q_V$ = 2.67 C/m$^3$ (σ), and (iv) $d$ = 116 μm, $u_{inj} \approx$ 15 m/s and $Q_V$ = 3.16 C/m$^3$ (υ).

## CONCLUSIONS

The general spray characteristics on charged sprays of viscous insulating liquids generated by charge injection atomizers have been investigated and extend the studies of Shrimpton and Yule [2, 11]. The liquid physical properties over the very small range we have looked at (for $780 \le \rho \le 815$ kg/m$^3$, $0.0008 \le \mu \le 0.0026$ kg/ms, $0.0225 \le \sigma_T \le 0.0250$ Ns/m$^2$) do not have much effect on the droplet radial dispersion rates, and this effect could be discounted when analyzing the charge-to-mass ratio. The annular mass flow rate at $r/d > 100$ sharply reduces suggesting that although highly charged drops exist outside this spray cone, they are small and possess the largest charge-to-mass ratios, and therefore be deflected most by a given electric field.

## ACKNOWLEDGMENTS

Acknowledgements are due to Oxford Laser (UK) Ltd. for helping to laser-drill the nozzle orifice, Esso Research (UK) Ltd. for supplying the diesel fuel, Engineering and Physical Sciences Research Council, UK for their financial support, and Ministry of Science, Technology and Environment, Malaysia for their sponsorship.

## REFERENCES

[1] A.R.H. Rigit and J.S. Shrimpton, Electrical Performance of Charge Injection Atomizers, submitted to *Atomization and Sprays*, 2003.

[2] J.S. Shrimpton and A.J. Yule, Atomization, Combustion and Control of Charged Hydrocarbon Sprays, *Atomization and Sprays*, vol. 11, pp. 365-396, 2001.

[3] C.P. Bankston, L.H. Back, E.Y. Kwack and A.J. Kelly, Experimental Investigation of Electrostatic Dispersion and Combustion of Diesel Fuel Jets, *J. Eng. Gas Turbine and Power*, vol. 110, pp. 361-368, 1988.

[4] R.J. Turnbull, On the Instability of an Electrostatically Sprayed Liquid Jet, *Trans. IEEE Ind. Appl.*, vol. 28, pp. 1432-1438, 1989.

[5] A.A. Naqwi, In Situ Measurement of Submicron Droplets in Electrosprays Using a Planar Phase Doppler System, *J. Aerosol Sci.*, vol. 25, pp. 1201-1211, 1994.

[6] P.F. Dunn and S.R. Snarski, Droplet Diameter, Flux, and Total Current Measurements in an Electrohydrodynamic Spray, *J. Appl. Phys.*, vol. 71, pp. 80-84, 1992.

[7] A. Gomez and K. Tang, On the Structure of an Electrostatic Spray of Monodisperse Droplets, *Phys. Fluids*, vol. 6, pp. 2317-2332, 1994.

[8] A. Gomez and K. Tang, Charge and Fission of Droplets in Electrostatic Sprays, *Phys. Fluids*, vol. 6, pp. 404-414, 1994.

[9] G. Gomez and K. Tang, Monodisperse Electrosprays of Low Electric Conductivity Liquids in the Cone-jet Mode, *J. Coll. Int. Sci.*, vol. 184, pp. 500-511, 1996.

[10] J.S. Shrimpton and A.J. Yule, Drop Size and Velocity Measurement in an Electrostatically Produced Hydrocarbon Spray, *J. Fluids Engineering*, vol. 120, pp. 580-585, 1998.

[11] J.S. Shrimpton and A.J. Yule, Characterization of Charged Hydrocarbon Sprays for Application in Combustion Systems, *Exp. Fluids*, vol. 26, pp. 460-469, 1999.

[12] J.H. Kim and T. Nakajima, Aerodynamic Influences on Droplet Atomization in an Electrostatic Spray, *JSME Int. Journal B*, vol. 42, pp. 224-229, 1999.

[13] J.S. Shrimpton and A.J. Yule, Electrohydrodynamics of Charge Injection Atomization: Regimes and Fundamental Limits, *Atomization and Spray*, vol. 13, pp. 46-63, 2003.

[14] J.S. Shrimpton, and A.J. Yule, Electrohydrodynamics of Charge Injection Atomization: Atomizer Design, accepted for publication, *Atomization and Spray*, 2001.

[15] Y. Hardalupas and J. Laker, Description of the Thermofluids Section 'Model 3' Phase Doppler Counter, Mechanical Engineering Department, Report TF/93/15, Imperial College London, 1993.

[16] Y. Hardalupas and A.M.K.P. Taylor, On the Measurement of the Particle Concentration Near a Stagnation Point, *Exp. Fluids*, vol. 8, pp. 113-118, 1989.